

DOI:10.1002/ejic.201402094

Zinc Metal–Organic Frameworks Based on a Flexible Benzylaminetetracarboxylic Acid and Bipyridine Colinkers

Chao Wang,^[a,b] Sifu Tang,^[a] Xiaoxia Lv,^[c] Liangjun Li,^[a,b] and Xuebo Zhao*^[a]

Keywords: Metal–organic frameworks / Zinc / Carboxylate ligands / Colinkers

Three new metal–organic frameworks (MOFs), $[\text{Zn}_2(\text{L})(\text{H}_2\text{O})] \cdot 3\text{DMF} \cdot 1.5\text{H}_2\text{O}$ (**1**), $[\text{Zn}_2(\text{L})(4,4'\text{-bpy})_{1.5}(\text{H}_2\text{O})_2] \cdot 2\text{DMF} \cdot 2\text{H}_2\text{O}$ (**2**), and $[\text{Zn}_2(\text{L})(2,2'\text{-bpy})_2(\text{DMF})_2] \cdot 2\text{DMF} \cdot 4\text{H}_2\text{O}$ (**3**) [$\text{H}_4\text{L} = 5,5'-(2,3,5,6\text{-tetramethyl-1,4-phenylene})\text{bis}(\text{methylene})\text{bis}(\text{azanediy})\text{diisophthalic acid}$, $4,4'\text{-bpy} = 4,4'\text{-bipyridine}$, $2,2'\text{-bpy} = 2,2'\text{-bipyridine}$, $\text{DMF} = N,N\text{-dimethylformamide}$], were synthesized under solvothermal conditions and characterized by single-crystal X-ray diffraction analysis, elemental analysis, IR spectroscopy, powder X-ray diffraction (PXRD), and thermogravimetric analysis (TGA). The L^{4-} ligands in **1–3** display different coordination modes, and the introduction of bipyridine colinkers brings significant struc-

tural variation into the frameworks. Complex **1** is constructed from dinuclear carboxylate $[\text{Zn}_2\text{O}(\text{COO})_4]$ secondary building units (SBUs) and H_4L ligands and exhibits a binodal (4,4)-connected pts net with 54.6% solvent-accessible void. Complex **2** exhibits an unprecedented tetranodal (3,4,4,4)-connected net, which is constructed from two types of crystallographically independent Zn^{II} ions, H_4L ligands, and the 4,4'-bipyridine colinker. Complex **3** is constructed from parallel 1D molecular ladders stacked along the *a* axis that generate 1D channels ($7.8 \times 10.4 \text{ \AA}$) and are hydrogen bonded to form 2D layers. The thermal stabilities and luminescence properties of **1–3** have also been studied in detail.

Introduction

From the concept of “nodes and spacers”^[1] to the strategy of “reticular chemistry”,^[2] the feasibility of the foresight design of metal–organic frameworks (MOFs) has established a compelling rationale to target MOFs for specific applications such as gas storage and separation, catalysis, luminescence, sensing, microelectronics, and optics.^[3] The underlying structures obtained from given secondary building units (SBUs) with polytopic linkers can be analyzed from the crystallographic and topological perspective.^[4] The selection of different metal centers and organic linkers can give rise to considerable structural diversity.^[5] Even for a given metal center and ligand, the resulting MOFs can possess varied structures and topologies under different reaction conditions, such as reactant ratio and concentration, pH value, solvent type and composition, and multiple ligand ratios.^[6] Another strategy to achieve structural diversity is the incorporation of flexible linkers into the framework; thus, the linkers possess conformational freedom

when coordinated to metal centers.^[7] Generally, this flexibility in MOFs manifests two forms, that is, varied coordination geometries between the metal center and ligand or free motion of the framework, such as reversible rotation and bending.^[7b,8] Additionally, the promising “mixed-ligand strategy” has been widely used to design and construct MOFs with desired and diverse structures and properties.^[6c,6e,6f,9]

On the basis of these considerations, a benzylamine-based tetracarboxylate ligand, 5,5'-(2,3,5,6-tetramethyl-1,4-phenylene)bis(methylene)bis(azanediy)diisophthalic acid (H_4L), has been designed and employed in the construction of MOFs with various architectures. H_4L has two terminal isophthalic acid units linked by the central benzylamine fragment. Four methyl groups are grafted onto the central benzene ring to enhance the steric hindrance of the whole ligand and ensure that the zygomorphic isophthalate groups are roughly in the same plane. Bipyridine colinkers are adopted to extend the structures constructed from Zn^{II} ions and H_4L . We successfully applied the above strategy and obtained three new MOFs, namely, $[\text{Zn}_2(\text{L})(\text{H}_2\text{O})] \cdot 3\text{DMF} \cdot 1.5\text{H}_2\text{O}$ (**1**), $[\text{Zn}_2(\text{L})(4,4'\text{-bpy})_{1.5}(\text{H}_2\text{O})_2] \cdot 2\text{DMF} \cdot 2\text{H}_2\text{O}$ (**2**, $4,4'\text{-bpy} = 4,4'\text{-bipyridine}$, $\text{DMF} = N,N\text{-dimethylformamide}$), and $[\text{Zn}_2(\text{L})(2,2'\text{-bpy})_2(\text{DMF})_2] \cdot 2\text{DMF} \cdot 4\text{H}_2\text{O}$ (**3**, $2,2'\text{-bpy} = 2,2'\text{-bipyridine}$). Their structures vary from a 3D (4,4)-connected pts network to a 3D twofold-interpenetrated (3,4,4,4)-connected framework and a 2D layer. Their syntheses, crystal structures, thermal stabilities, and photoluminescence properties are reported herein.

[a] Qingdao Institute of Bioenergy and Bioprocess Technology, Chinese Academy of Sciences, Shandong 266101, China
E-mail: zhaorb@qibebt.ac.cn
<http://info.qibebt.cas.cn/hydrogen/6.htm>

[b] University of Chinese Academy of Sciences, Beijing, China

[c] School of Chemistry and Chemical Engineering, Qufu Normal University, Qufu, China

Supporting information for this article is available on the WWW under <http://dx.doi.org/10.1002/ejic.201402094>.

Results and Discussion

Structure of $[\text{Zn}_2(\text{L})(\text{H}_2\text{O})]\cdot 3\text{DMF}\cdot 1.5\text{H}_2\text{O}$ (**1**)

Complex **1** crystallizes in the monoclinic space group $C2/c$, and the asymmetric unit contains one Zn^{II} ion, half of an L^{4-} anion, and half of a bridging aqua ligand. The Zn^{II} ion is surrounded by four oxygen atoms from three different carboxylate groups of three L^{4-} ligands [$\text{Zn}-\text{O}$ 1.912(3), 1.974(3), and 2.001(3) Å] and one terminal aqua ligand [$\text{Zn}-\text{O}$ 1.935(3) Å] to generate a distorted tetrahedral coordination geometry (Figure 1, a). Two Zn^{II} atoms are connected by two carboxylate bridges from two different L^{4-} anions and one bridging oxygen atom to form a dinuclear carboxylate $[\text{Zn}_2\text{O}(\text{COO})_4]$ SBU [$\text{Zn}\cdots\text{Zn}$ 3.0005(8) Å; Figure 1, b]. Each SBU bridges four L^{4-} anions and serves as a distorted 4-connected node. Each L^{4-} ligand links six Zn^{II} ions with its four carboxylate groups, which are located symmetrically around the center of the L^{4-} ligand and display monodentate bridging and bidentate chelate coordination modes (Figure 1, c). Notably, the two isophthalate units of the L^{4-} ligand are almost parallel and form a square-planar topological node (Figure 1, c). Thus, the whole net of **1** can be rationalized as a binodal (4,4)-connected pts net with the same $(4^2\cdot 8^4)$ point symbols (Figure 1, d)^[10] but with the different long vertex symbols of $[4.4.8_2.8_2.8_8.8_8]$ and $[4.4.8_7.8_7.8_7.8_7]$ for L^{4-} and the dinuclear SBU, respectively. The framework generated by the construction of $[\text{Zn}_2\text{O}(\text{COO})_4]$ SBUs and L^{4-} exhibits one-dimensional (1D) channels along the crystallographic $[10\bar{1}]$ and $[110]$ directions, respectively (Figure 1, e and f). The

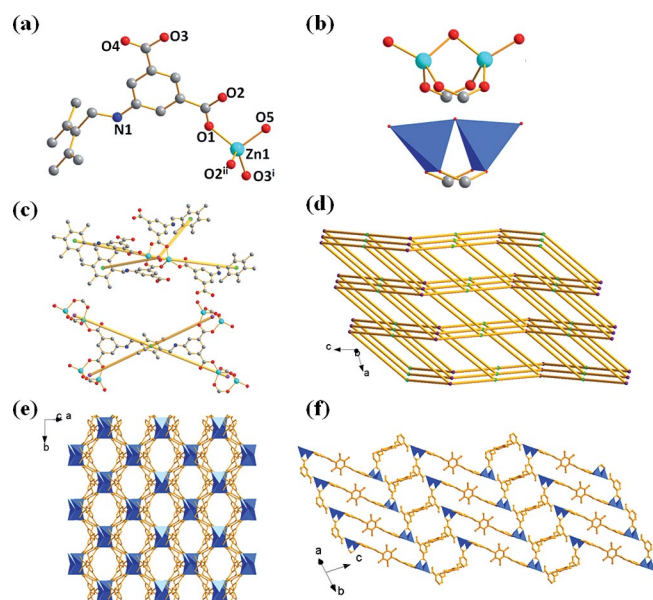


Figure 1. (a) The coordination environment of the Zn^{II} atoms in **1** [symmetry codes: (i) $x - 1/2, y + 1/2, z$; (ii) $-x, y, -z + 1/2$]. (b) $[\text{Zn}_2\text{O}(\text{COO})_4]$ SBU in **1**. (c) $[\text{Zn}_2\text{O}(\text{COO})_4]$ SBU and L^{4-} ligand as tetrahedral and square-planar 4-connected nodes, respectively. (d) (4,4)-connected pts net topology in **1**. (e,f) Channels along the crystallographic $[10\bar{1}]$ and $[110]$ directions, respectively.

solvent-accessible void of **1** was calculated by PLATON^[11] analysis as 54.6% of the crystal volume (2670.4 out of the 4892.5 Å³ unit cell volume).

Structure of $[\text{Zn}_2(\text{L})(4,4'\text{-bpy})_{1.5}(\text{H}_2\text{O})_2]\cdot 2\text{DMF}\cdot 2\text{H}_2\text{O}$ (**2**)

Single-crystal X-ray diffraction analysis revealed that **2** crystallizes in the triclinic space group $P\bar{1}$, and the asymmetric unit consists of two Zn^{II} ions (Zn1 and Zn2), one L^{4-} ligand, one and a half 4,4'-bpy ligands, and two coordinated water molecules. The two crystallographically independent Zn^{II} ions, Zn1 and Zn2 , are five- and four-coordinate, respectively (Figure 2, a). Each Zn1 atom is five-coordinate to two oxygen atoms from two L^{4-} anions, two nitrogen atoms of two 4,4'-bpy molecules, and one aqua ligand to form a trigonal-bipyramidal coordination geometry [$\text{Zn1}-\text{N2}$ 2.080(3), $\text{Zn1}-\text{O1}$ 1.978(3), $\text{Zn1}-\text{O4}^{\text{i}}$ 1.969(3), $\text{Zn1}-\text{N3}$ 2.274(4), $\text{Zn1}-\text{O5}$ 2.120(3)]. Similarly to Zn1 , each Zn2 atom is bonded to two L^{4-} ligands, one H_2O molecule, and only one bpy ligand without the perpendicular bpy ligand that connects two layers [$\text{Zn2}-\text{N1}$ 2.046(3), $\text{Zn2}-\text{O7}$ 1.951(3), $\text{Zn2}-\text{O9}^{\text{ii}}$ 1.914(3), $\text{Zn2}-\text{O6}$ 2.016(3); Figure 2, a]. Each L^{4-} ligand links four Zn1 or Zn2 centers; the four carboxylate groups are located symmetrically around the center of the L^{4-} ligand and all display a monodentate coordination mode (Figure 2, b). Importantly, in the two crystallographically independent L^{4-} ligands, both isophthalate units are almost parallel and form a square-planar topological node, and the two types of L^{4-} nodes combine with 4-connected Zn1 and 3-connected Zn2 nodes to generate the 3D framework (Figure 2, c). From a topological point of view, the resulting 3D net relies on the construction of tetrahedral Zn1 , tetrahedral Zn2 , and two types of square-planar L^{4-} building units, which serve as 3-, 4-, 4-, and 4-connected nodes, respectively (Figure 2, b). Thus, the whole 3D framework can be rationalized as a new 4-nodal $(3,4,4,4)$ -connected net (Figure 2, c) with the Schläfli symbol $(4\cdot 6^2)(4\cdot 6^4\cdot 8)(4^2\cdot 6^4\cdot 8^2)$.

A detailed analysis shows that the framework structure of **2** is twofold-interpenetrated and consists of two identical crystallographically independent networks. For a single network, each 2D layer is linked to the adjacent layers by bpy linkers and is offset from two adjacent layers, which results in the loss of porosity along the b axis (Figure 2, d and e). The two networks are related to each other by a translation of 14.72 Å along the b axis. Each single network consists of infinite honeycomb 2D layers with hexagonal cavities, which consist of a chain of Zn^{II} ions bridged by L^{4-} and bpy linkers (Figure 2, f). The layers are further connected by bpy linkers through $\text{Zn}-\text{N}$ bonding interactions to form a three-dimensional (3D) coordination network with the brick-wall motif (Figure 2, g). Despite the unexpected occurrence of twofold interpenetration, complex **2** still possesses a solvent-accessible void space, calculated to be 761.1 Å³ by PLATON,^[11] that is, 29.7% of the lattice volume. In addition, the 3D framework is reinforced by $\text{O}_{\text{water}}\cdots\text{H}\cdots\text{O}_{\text{carboxylate}}$, $\text{C}_{\text{L}^{4-}}\cdots\text{H}\cdots\text{O}_{\text{carboxylate}}$, $\text{C}_{\text{bpy}}\cdots\text{H}\cdots\text{O}_{\text{carboxylate}}$

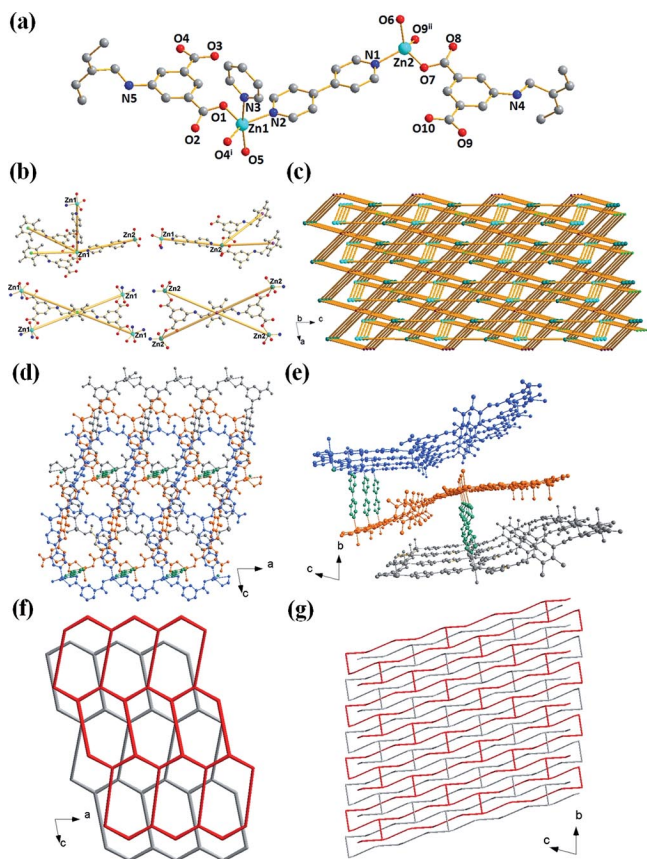


Figure 2. (a) The coordination environments of the Zn^{II} ions in **2** [symmetry codes: (i) $x - 1, y, z$; (ii) $x + 1, y, z$]. (b) Four types of node in **2**. (c) (3,4,4,4)-connected net topology in **2**. (d, e) Adjacent layers of a single network viewed along the b and a axes, respectively. (f) Simplified adjacent layers of the two independent networks viewed along the b axis. (g) Simplified view of the two independent networks in **2**.

and $C_{L4}-H\cdots N_{L4}$ hydrogen bonds [2.629(4) to 3.295(7) Å] among coordinated water molecules, L^4 ligands, 4,4'-bpy ligands, and carboxylate groups (Table S2).

Structure of $[Zn_2(L)(2,2'\text{-bpy})_2(\text{DMF})_2]\cdot 2\text{DMF}\cdot 4\text{H}_2\text{O}$ (**3**)

In comparison to that of **2**, the framework structure of **3** shows some crystallographic similarities. Complex **3** also crystallizes in the triclinic space group $P\bar{1}$, and the asymmetric unit consists of one Zn^{II} ion (Zn1), half of an L^4 ligand, one 2,2'-bpy ligand, and one coordinated DMF molecule. Each Zn²⁺ ion is six-coordinate through binding to the O and N atoms from one chelated carboxylate group, one monodentate carboxylate group, one chelate 2,2'-bpy ligand, and one DMF molecule to form a distorted octahedral geometry (Figure 3, a). Complex **3** is assembled from 1D molecular ladders that generate 1D channels (Figure 3, b). The Zn^{II} ions are linked by L^4 ions to generate a 1D ladder-type structure that is elongated along the b axis, and all of the 1D molecular ladders are stacked in a parallel way (Figure 3, c). The distance between two adjacent 1D molecular ladders along the b axis is 9.000 Å. Each rectan-

gular cavity in the ladder is $7.8 \times 10.4 \text{ \AA}^2$ and is constructed from two Zn²⁺ ions (Zn \cdots Zn 16.862 Å) and two L^4 ligands. The shortest Zn \cdots Zn distance along the b axis is 10.197 Å. Interestingly, the ladders are connected to form 2D layers through $C_{\text{bpy}}-H\cdots O_{\text{carboxylate}}$ hydrogen bonds, which provide additional stability to the structure (Figure 3, d and Table S3). The lattice water and DMF molecules occupy the cavities within the ladders and interact with the framework through hydrogen bonds. In addition, intermolecular hydrogen bonds are also observed in the framework (Table S3).

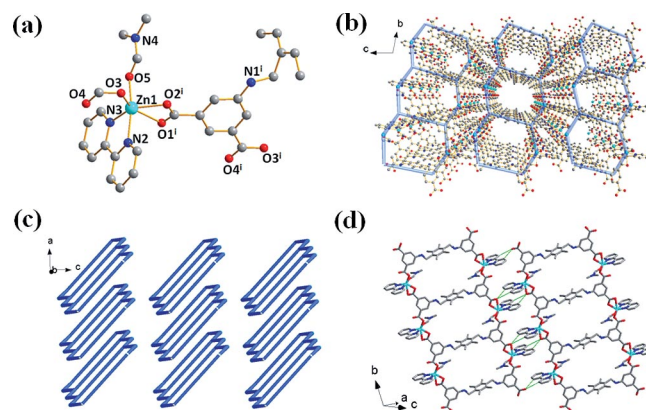


Figure 3. (a) The coordination environments of the Zn^{II} ions in **3** [symmetry code: (i) $x, y - 1, z$]. (b) 1D molecular ladders along the b axis and 1D channels along the a axis. (c) The parallel 1D molecular ladders stacked along the a axis. (d) The 2D layer constructed from 1D ladders through hydrogen bonds (green lines represent hydrogen bonds).

Configurations of L^4 , Coordination Modes, and Effects of Bipyridine Colinkers

With the introduction and variation of the auxiliary ligand, the tetracarboxylate ligand H_4L shows different coordination modes and three new MOFs with different topologies are formed. In **1**, dinuclear carboxylate $[Zn_2O(\text{COO})_4]$ SBUs are formed as the four carboxylate groups of L^4 link six Zn^{II} ions through a mixed bridging-bidentate and monodentate coordination mode (Figure 4). In **2**, the pyridyl N atoms of 4,4'-bpy replace some of the coordination sites previously occupied by the L^4 ligand, which results in the μ_4-O, O', O'', O''' coordination mode. Furthermore, the lengthened asymmetric unit leads to the emergence of the twofold-interpenetrated framework. In **3**, both N atoms of one 2,2'-bpy ligand participate in the coordination to the Zn^{II} ions and inhibit the growth of the network to a higher dimensionality. The L^4 ligand in **3** presents two types of coordination mode, namely, monodentate and chelating-bidentate. By comparison, we found that the introduction of different bipyridine colinkers can thoroughly change the whole structure of the MOF, including the coordination mode, dimensionality, and number of independent networks.

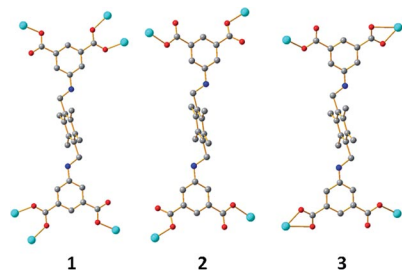


Figure 4. Coordination modes of the L^{4-} ligands in 1–3.

The flexible $-\text{CH}_2\text{NH}-$ spacer can give rise to various configurations in MOFs.^[12i] However, the four methyl groups grafted onto the central benzene ring effectively enhance the steric hindrance of the whole ligand and result in a similar configuration of the L^{4-} ligands in 1–3, that is, the zygomorphic isophthalate groups are roughly in the same plane. Despite a higher steric hindrance in the L^{4-} ligand, the whole framework still possess some degree of flexibility owing to the rotatable $-\text{CH}_2\text{NH}-$ spacer. Specifically, the plane angles between the terminal benzene rings and the central one of the L^{4-} ligands in 1–3 shows certain differences and are 84.908° for 1, 83.240° for 2, and 78.055° for 3. Furthermore, the $-\text{CH}_2-\text{NH}-$ angles also exhibit differences for 1–3 (Table S1).

Thermal Analyses

To investigate the thermal stabilities of 1–3, thermogravimetric analysis (TGA) was performed under a N_2 atmosphere, and the TGA profiles are shown in Figure 5. For 1, the TGA profile shows a weight loss between 30 and 96°C , which is attributed to the loss of one and a half lattice water molecules (found/calcd. 2.82/2.96%). The second weight loss step between 96 and 270°C corresponds to the loss of three lattice DMF molecules (found/calcd. 25.5/24.0%); the subsequent weight loss between 270 and 404°C (8.59%) is due to the partial decompositions of the framework. Above 404°C , complex 1 starts to decompose rapidly. For 2, the TGA profile shows a multistep weight loss between 30 and 145°C on account of the loss of two lattice water molecules, two DMF molecules, and two coordinated water molecules (found/calcd 18.7/19.2%). The framework is stable to 257°C with a minor weight loss (2.8%). Another weight loss step between 257 and 425°C (9.2%) corresponds to the partial decomposition of the L^{4-} and bpy ligands. Above 425°C , complex 2 starts to decompose rapidly. The TGA profile of 3 shows a multistep weight loss between 30 and 199°C , which corresponds to the loss of four lattice water molecules, two lattice DMF molecules, and two coordinated DMF molecules, followed by a gradual weight loss between 199 and 250°C . Above 250°C , complex 3 starts to decompose rapidly. All of the complexes formed white zinc oxide powder after the TGA analyses.

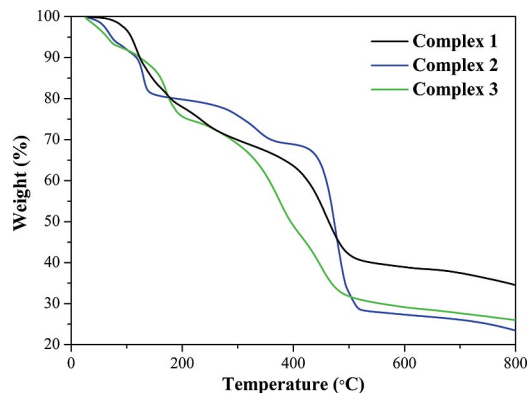


Figure 5. TGA profiles of 1–3.

Luminescence Properties

The photoluminescence properties of the Zn-based MOFs have been widely studied, in consideration of their potential applications as functional luminescent materials.^[12,9d] The photoluminescence spectra of solid samples of ligands H_4L , 2,2'-bpy, and 4,4'-bpy and complexes 1–3 were investigated at ambient temperature in the visible region (Figure 6 and Table S4). For the free ligands H_4L , 2,2'-bpy, and 4,4'-bpy, emission peaks were observed at 452 ($\lambda_{\text{ex}} = 340\text{ nm}$), 544 ($\lambda_{\text{ex}} = 340\text{ nm}$), and 429 nm ($\lambda_{\text{ex}} = 346\text{ nm}$), respectively, and are attributed to the $\pi^* \rightarrow \pi$ or $\pi^* \rightarrow n$ transitions. Compared with those of the free ligands H_4L , 2,2'-bpy, and 4,4'-bpy, apparent blue- or redshifts of the emission bands for 1–3 can be observed, and the maximum emission wavelengths are 420 nm ($\lambda_{\text{ex}} = 350\text{ nm}$) for 1, 602 nm ($\lambda_{\text{ex}} = 380\text{ nm}$) for 2, and 524 nm ($\lambda_{\text{ex}} = 334\text{ nm}$) for 3. The emission of 1 is tentatively assigned to the intraligand transition of the L^{4-} ligand, whereas the emissions of 2 and 3 may be a mixture with characteristics of intraligand and ligand-to-ligand charge transfer (LLCT) transitions, as the Zn^{II} ion is difficult to oxidize or reduce owing to its d^{10} configuration.^[13,12g] The observed red- or blueshift of the emission maxima between the complexes and ligands are considered to mainly arise from the different coordination

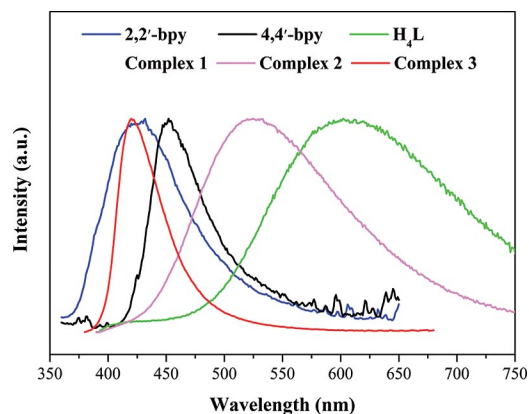


Figure 6. Solid-state emission spectra of 2,2'-bpy, 4,4'-bpy, H_4L , and 1–3.

modes of the ligands to the Zn^{II} ions and the coordination environments around the Zn^{II} ions. The redshift of the emission band for **2** compared with those of **1** and **3** might be ascribed to the employment of the 4,4'-bpy linker, which can expand the π -conjugation system and consequently enhance the delocalization of electron density from the ligand to the metal and reduce the energy gap between the π^* - π molecular orbital of the ligands.

Conclusions

Three new zinc metal-organic frameworks constructed from a flexible benzylaminetetra-carboxylic acid and bipyridine colinkers have been successfully obtained under solvothermal conditions. With the introduction of different bipyridine colinkers, complexes **1–3** display diverse structural features including a 3D (4,4)-connected pts network constructed from [Zn₂O(COO)₄] SBUs (**1**), a new twofold-interpenetrated (3,4,4,5)-connected framework (**2**), and a 2D layer constructed from 1D molecular ladders through hydrogen bonds (**3**). The various coordination modes of the L⁴⁻ anion reveal that the presence of bipyridine colinkers greatly influences the construction of coordination complexes. The diverse structural features also engender different photoluminescence properties.

Experimental Section

Materials and Methods: All reagents and solvents were commercially available and used without further purification. The ¹H NMR spectra were recorded with a Bruker AVANCE III (600 MHz) spectrophotometer. The elemental analyses for C, H, and N were performed with an Elementar Vario EL III elemental analyzer. The infrared (IR) spectra were acquired with a Thermo Fisher Nicolet 6700 FTIR spectrometer. The powder X-ray diffraction (PXRD) measurements were performed with a Bruker AXS D8 Advance $\theta/2\theta$ diffractometer equipped with a Cu-K α radiation source ($\lambda = 1.5418 \text{ \AA}$) at a scan speed of 2° min^{-1} and a step size of 0.02° in 2θ at room temperature. The thermogravimetric analyses (TGA) were performed in the temperature range 30–800 °C with a NETZSCH STA449 F3 TG-DSC analyzer under a flow of nitrogen (20 mL min^{-1}) at a ramp rate of $10^\circ \text{ C min}^{-1}$. The luminescence spectra of the solid samples were recorded with a HORIBA Jobin Yvon FluoroMax-4 fluorescence spectrometer.

Diethyl 5-Aminoisophthalate: 5-Aminoisophthalic acid (18.12 g, 0.1 mol) was dissolved in ethanol (200 mL), and then concentrated H₂SO₄ (20 mL) was added. After that, the solution was stirred under reflux for 12 h at 100 °C. The pH value was adjusted to 7.0 by using 10 wt.-% Na₂CO₃ aqueous solution, and the solution was filtered. The solvent was removed from the filtrate with a rotary evaporator, and the crude product was extracted with diethyl ether. The organic layer was then dried with Na₂SO₄, and the solvent was removed with a rotary evaporator. The resulting product was dried under vacuum at 65 °C (19.50 g, 82%).

1,4-Bis(bromomethyl)-2,3,5,6-tetramethylbenzene: 1,2,4,5-Tetramethylbenzene (13.44 g, 0.1 mol) and paraformaldehyde (6.00 g, 0.2 mol) were added to an aqueous solution (60 mL) of HBr/HOAc (33 wt.-%), and the mixture was stirred at 85 °C till a white solid precipitate was observed. The solution was kept at 85 °C for 20 min

and then heated to 95 °C for 12 h. After that, deionized water (100 mL) was added to the above solution. The resulting product was collected by filtration, washed with deionized water, and air-dried at 65 °C (26.50 g, 83%).

Tetraethyl 5,5'-(2,3,5,6-Tetramethyl-1,4-phenylene)bis(methylene)bis(azanediy)diisophthalate [(Et)₄L]: Diethyl 5-aminoisophthalate (7.12 g, 0.03 mol) was dissolved in acetonitrile (100 mL), followed by the addition of K₂CO₃ (5.53 g, 0.04 mol). Then, the solution was cooled to less than 10 °C in an ice-water bath prior to the dropwise addition of 1,4-bis(bromomethyl)-2,3,5,6-tetramethylbenzene (4.80 g, 0.015 mol, in 150 mL acetonitrile). After the addition, the solution was kept below 10 °C for 1 h and stirred for 16 h at room temperature. The solvent was removed under vacuum. After that, the crude product was extracted with CHCl₃ and washed with H₂O several times. The organic layer was then dried with Na₂SO₄, and the solvent was removed with a rotary evaporator. The resulting product was dried under vacuum at 65 °C (6.20 g, 65%). ¹H NMR (600 MHz, CDCl₃): $\delta = 8.05$ (s, 2 H), 7.50 (s, 4 H), 4.40 (m, 8 H), 4.34 (d, 4 H), 3.76 (s, 2 H), 2.32 (s, 12 H), 1.41 (t, 12 H) ppm.

5,5'-(2,3,5,6-Tetramethyl-1,4-phenylene)bis(methylene)bis(azanediy)diisophthalic Acid (H₄L): A NaOH (2 M) aqueous solution (150 mL) was added to a solution of (Et)₄L (6.20 g, 0.0098 mmol) in methanol/tetrahydrofuran (MeOH/THF, 1:1 v/v; 200 mL), and the solution was stirred under reflux for 24 h at 100 °C. The organic solvent was removed with a rotary evaporator at 65 °C. The pH value was adjusted to 3–4 with concentrated HCl, and a large amount of pale yellow precipitated appeared. The resulting solution was cooled overnight at 5 °C. The resulting pale yellow precipitated was collected by filtration, washed with water and diethyl ether, and then dried under vacuum at 65 °C (4.85 g, 95%). ¹H NMR [600 MHz, (CD₃)₂SO]: $\delta = 12.96$ (s, 4 H), 7.73 (s, 2 H), 7.49 (d, 2 H), 6.11 (s, 2 H), 4.19 (s, 4 H), 2.25 (s, 12 H) ppm. IR (KBr): $\tilde{\nu} = 3409$ (b), 2923 (w), 1711 (w), 1682 (m), 1606 (s), 1508 (w), 1428 (w), 1382 (w), 1297 (w), 1262 (m), 1210 (w), 1096 (w), 992 (w), 798 (w), 762 (m), 674 (m) cm⁻¹.

[Zn₂(L)(H₂O)]·3DMF·1.5H₂O (1**):** A mixture of Zn(NO₃)₆·6H₂O (0.059 g, 0.2 mmol), H₄L (0.052 g, 0.1 mmol), H₂O (2 mL), and DMF (10 mL) was stirred for 30 min in air. The solution was placed in a Teflon-lined stainless steel vessel (25 mL), which was sealed and heated to 100 °C for 24 h. Cooling the vessel to room temperature gave colorless crystals (0.031 g), yield 34% (based on Zn). C₃₇H₅₁N₅O_{13.5}Zn₂ (912.64): calcd. C 48.69, H 5.63, N 7.67; found C 48.45, H 5.54, N 7.79. IR (KBr): $\tilde{\nu} = 3424$ (b), 2927 (w), 1659 (s), 1578 (s), 1497 (w), 1420 (m), 1384 (m), 1282 (w), 1249 (w), 1142 (w), 1099 (m), 1064 (w), 1024 (w), 997 (w), 840 (w), 780 (s), 727 (s), 662 (w) cm⁻¹.

[Zn₂(L)(4,4'-bpy)_{1.5}(H₂O)₂]·2DMF·2H₂O (2**):** A mixture of Zn(NO₃)₆·6H₂O (0.059 g, 0.2 mmol), H₄L (0.052 g, 0.1 mmol), 4,4'-bipyridine (0.016 g, 0.1 mmol), H₂O (3 mL), and DMF (9 mL) was stirred for 30 min in air. The solution was placed in a Teflon-lined stainless steel vessel (25 mL), which was sealed and heated to 100 °C for 24 h. Yellow plate crystals of **2** were collected (0.056 g) in 51% yield (based on Zn). C₄₉H₅₆N₇O₁₄Zn₂ (1097.83): calcd. C 53.61, H 5.14, N 8.93; found C 53.72, H 5.20, N 8.78. IR (KBr): $\tilde{\nu} = 3424$ (b), 2925 (w), 1672 (s), 1611 (m), 1564 (s), 1492 (m), 1421 (m), 1384 (s), 1323 (w), 1280 (w), 1254 (w), 1227 (m), 1143 (w), 1093 (m), 1072 (m), 1046 (w), 1013 (w), 817 (m), 782 (s), 732 (s), 662 (w), 638 (m) cm⁻¹.

[Zn₂(L)(2,2'-bpy)₂(DMF)₂]·2DMF·4H₂O (3**):** The preparation of **3** was similar to that of **2**, except that 2,2'-bipyridine (0.016 g, 0.1 mmol) was used instead of 4,4'-bipyridine. Yellow plate crystals

Table 1. Crystal data and structure refinements for 1–3.

| | Complex 1 | Complex 2 | Complex 3 |
|---|---|--|--|
| Empirical formula | C ₁₄ H ₁₃ NO _{4.50} Zn | C ₄₃ H ₃₈ N ₅ O ₁₀ Zn ₂ | C ₃₀ H ₃₈ N ₅ O ₈ Zn |
| Formula weight | 332.62 | 915.52 | 662.02 |
| Temperature [K] | 173(2) | 293(2) | 173(2) |
| Wavelength [Å] | 0.71073 | 0.71073 | 0.71073 |
| Crystal system | monoclinic | triclinic | triclinic |
| Space group | C2/c | P $\bar{1}$ | P $\bar{1}$ |
| a [Å] | 15.8430(9) | 9.572(2) | 9.000(3) |
| b [Å] | 11.3621(6) | 14.718(4) | 10.197(3) |
| c [Å] | 28.2091(18) | 19.571(5) | 18.109(4) |
| α [°] | 90 | 73.658(3) | 100.459(7) |
| β [°] | 105.531(2) | 77.093(3) | 90.851(9) |
| γ [°] | 90 | 80.260(3) | 106.781(8) |
| V [Å ³] | 4892.5(5) | 2562.2(11) | 1560.7(7) |
| Z | 8 | 2 | 2 |
| D _{calcd.} [g cm ⁻³] | 0.903 | 1.187 | 1.409 |
| Absorption coefficient [mm ⁻¹] | 1.013 | 0.988 | 0.844 |
| F(000) | 1360 | 942 | 694 |
| Crystal size [mm] | 0.10 × 0.10 × 0.10 | 0.20 × 0.20 × 0.10 | 0.26 × 0.24 × 0.20 |
| θ range for data collection [°] | 3.41 to 25.00 | 2.03 to 25.00 | 1.15 to 27.52 |
| Limiting indices | -18 < h < 18 -13 < k < 13 -33 < l < 33 | -11 < h < 11 -17 < k < 16 -23 < l < 23 | -11 < h < 11, -13 < k < 12, 0 < l < 23 |
| Reflections collected/unique | 16575/4244 [R(int) = 0.0498] | 17944/8867 [R(int) = 0.0600] | 4901/4901 [R(int) = 0.0000] |
| Completeness to $\theta = 25.00$ [%] | 98.3 | 98.1 | 67.1 |
| Absorption correction | semi-empirical from equivalents | semi-empirical from equivalents | semi-empirical from equivalents |
| Max. and min. transmission | 0.9055 and 0.9055 | 0.9076 and 0.8268 | 0.8493 and 0.8104 |
| Refinement method | full-matrix least squares on F ² | full-matrix least squares on F ² | full-matrix least squares on F ² |
| Data/restraints/parameters | 4244/6/187 | 8867/4/546 | 4901/13/364 |
| Goodness-of-fit on F ² | 0.971 | 1.083 | 1.049 |
| R ₁ , ^[a] wR ₂ ^[b] [I > 2 σ (I)] | 0.0553, 0.1453 | 0.0611, 0.1054 | 0.0767, 0.2101 |
| R ₁ , ^[a] wR ₂ ^[b] (all data) | 0.0846, 0.1591 | 0.0964, 0.1132 | 0.1037, 0.2398 |
| Largest diff. peak, hole [e Å ⁻³] | 0.613, -0.415 | 1.188, -0.767 | 0.773, -0.647 |

[a] $R_1 = \sum ||F_o| - |F_c|| / \sum |F_o|$. [b] $wR_2 = [\sum w(F_o^2 - F_c^2)^2 / \sum w(F_o^2)^2]^{1/2}$.

of **3** were collected (0.050 g) in 38% yield (based on Zn). C₆₀H₇₆N₁₀O₁₆Zn₂ (1324.04): calcd. C 54.42, H 5.79, N 10.58; found C 53.37, H 5.68, N 10.44. IR (KBr): $\tilde{\nu}$ = 3431 (b), 2926 (w), 1660 (s), 1621 (s), 1579 (m), 1494 (w), 1474 (w), 1442 (w), 1416 (w), 1386 (w), 1364 (w), 1257 (w), 1100 (m), 1059 (w), 1022 (w), 780 (s), 769 (s), 736 (w), 721 (w), 661 (w) cm⁻¹.

Crystallography: The single-crystal X-ray diffraction data were collected with a Bruker Smart CCD diffractometer by using the ω -scan method with graphite-monochromated Mo-K α radiation (λ = 0.71073 Å) at 293 K. Absorption corrections were applied by using the multiscan technique. The structures were solved by direct methods and developed by difference Fourier techniques with the SHELXTL software package.^[14] The SQUEEZE routine implemented in PLATON^[15] was used to remove the highly disordered guest molecules in **1** and **2**. The crystal data as well as details of the data collection and refinement for **1–3** are summarized in Table 1, and selected bond lengths and angles are given in Table S1.

The experimental and simulated PXRD patterns of **1–3** are in good agreement, which indicates the phase purity of the complexes (Figure S4).

CCDC-977281 (for **1**), -977282 (for **2**), and -977283 (for **3**) contain the supplementary crystallographic data for this paper. These data can be obtained free of charge from The Cambridge Crystallographic Data Centre via www.ccdc.cam.ac.uk/data_request/cif.

Supporting Information (see footnote on the first page of this article): ¹H NMR spectra of (Et)₄L and H₄L, IR spectra of H₄L and **1–3**, PXRD patterns of **1–3**, and crystallographic data in CIF format.

Acknowledgments

This work was supported by grants from the National Natural Science Foundation of China (NSFC) (grant numbers 21073216 and 21173246) and the “Hundred-talent Project” (grant number KJXC2-YW-W34) of the Chinese Academy of Sciences.

- [1] a) B. F. Hoskins, R. Robson, *J. Am. Chem. Soc.* **1989**, *111*, 5962–5964; b) R. W. Gable, B. F. Hoskins, R. Robson, *J. Chem. Soc., Chem. Commun.* **1990**, 1677–1678; c) C. T. Chen, S. Suslick, *Coord. Chem. Rev.* **1993**, *128*, 293–322; d) M. Fujita, Y. J. Kwon, S. Washizu, K. Ogura, *J. Am. Chem. Soc.* **1994**, *116*, 1151–1152; e) M. Fujita, O. Sasaki, K. Y. Watanabe, K. Ogura, K. Yamaguchi, *New J. Chem.* **1998**, *22*, 189–191; f) S. Kawata, S. Kitagawa, M. Kondo, I. Furuchi, M. Munakata, *Angew. Chem. Int. Ed. Engl.* **1994**, *33*, 1759–1761; *Angew. Chem.* **1994**, *106*, 1851; g) L. Carlucci, G. Ciani, D. W. von Gundenberg, D. M. Proserpio, A. Sironi, *Chem. Commun.* **1997**, 631–632; h) K. Biradha, Y. Hongo, M. Fujita, *Angew. Chem. Int. Ed.* **2000**, *39*, 3843–3845; *Angew. Chem.* **2000**, *112*, 4001.
- [2] a) O. M. Yaghi, M. O’Keeffe, N. W. Ockwig, H. K. Chae, M. Eddaoudi, J. Kim, *Nature* **2003**, *423*, 705–714; b) N. W. Ockwig, O. Delgado-Friedrichs, M. O’Keeffe, O. M. Yaghi, *Acc. Chem. Res.* **2005**, *38*, 176–182; c) H. Furukawa, J. Kim, N. W. Ockwig, M. O’Keeffe, O. M. Yaghi, *J. Am. Chem. Soc.* **2008**, *130*, 11650–11661.
- [3] a) N. L. Rosi, J. Eckert, M. Eddaoudi, D. T. Vodak, J. Kim, M. O’Keeffe, O. M. Yaghi, *Science* **2003**, *300*, 1127–1129; b) M. P. Suh, H. J. Park, T. K. Prasad, D. W. Lim, *Chem. Rev.* **2012**, *112*, 782–835; c) K. Sumida, D. L. Rogow, J. A. Mason, T. M. McDonald, E. D. Bloch, Z. R. Herm, T. H. Bae, J. R. Long,

- Chem. Rev.* **2012**, *112*, 724–781; d) J. Liu, P. K. Thallapally, B. P. McGrail, D. R. Brown, J. Liu, *Chem. Soc. Rev.* **2012**, *41*, 2308–2322; e) J. R. Li, R. J. Kuppler, H. C. Zhou, *Chem. Soc. Rev.* **2009**, *38*, 1477–1504; f) J. R. Li, J. Sculley, H. C. Zhou, *Chem. Rev.* **2012**, *112*, 869–932; g) P. Nugent, Y. Belmabkhout, S. D. Burd, A. J. Cairns, R. Luebke, K. Forrest, T. Pham, S. Ma, B. Space, L. Wojtas, M. Eddaoudi, M. J. Zaworotko, *Nature* **2013**, *495*, 80–84; h) J. Lee, O. K. Farha, J. Roberts, K. A. Scheidt, S. T. Nguyen, J. T. Hupp, *Chem. Soc. Rev.* **2009**, *38*, 1450–1459; i) M. Yoon, R. Srirambalaji, K. Kim, *Chem. Rev.* **2012**, *112*, 1196–1231; j) S. R. Caskey, A. G. Wong-Foy, A. J. Matzger, *J. Am. Chem. Soc.* **2008**, *130*, 10870–0871; k) J. Cepeda, S. Pérez-Yáñez, G. Beobide, O. Castillo, M. Fischer, A. Luque, P. A. Wright, *Chem. Eur. J.* **2014**, *20*, 1554–1568; l) P. D. C. Dietzel, R. E. Johnsen, H. Fjellvag, S. Bordiga, E. Groppo, S. Chavan, R. Blom, *Chem. Commun.* **2008**, 5125–5127; m) Y. Cui, B. Chen, G. Qian, *Metal-Organic Frameworks for Photonics Applications*, Springer, Berlin/Heidelberg, Germany, **2014**, p. 1–26; n) P. Falcaro, S. Furukawa, *Angew. Chem. Int. Ed.* **2012**, *51*, 8431–8433; *Angew. Chem.* **2012**, *124*, 8557; o) Y. Cui, Y. Yue, G. Qian, B. Chen, *Chem. Rev.* **2012**, *112*, 1126–1162.
- [4] a) M. Eddaoudi, D. B. Moler, H. Li, B. Chen, T. M. Reineke, M. O’Keefe, O. M. Yaghi, *Acc. Chem. Res.* **2001**, *34*, 319–330; b) D. J. Tranchemontagne, J. L. Mendoza-Cortes, M. O’Keefe, O. M. Yaghi, *Chem. Soc. Rev.* **2009**, *38*, 1257–1283; c) S. Pérez-Yáñez, G. Beobide, O. Castillo, J. Cepeda, A. Luque, A. T. Aguayo, P. Román, *Inorg. Chem.* **2011**, *50*, 5530–5332.
- [5] a) D. Zhao, D. J. Timmons, D. Yuan, H. C. Zhou, *Acc. Chem. Res.* **2010**, *43*, 123–133; b) F. A. Paz, J. Klinowski, S. M. Vilela, J. P. Tome, J. A. Cavaleiro, J. Rocha, *Chem. Soc. Rev.* **2012**, *41*, 1088–1110; c) T. R. Cook, Y. R. Zheng, P. J. Stang, *Chem. Rev.* **2012**, *113*, 734–777.
- [6] a) Q. Gao, Y. B. Xie, J. R. Li, D. Q. Yuan, A. A. Yakovenko, J. H. Sun, H. C. Zhou, *Cryst. Growth Des.* **2012**, *12*, 281–288; b) D. Kim, X. Song, J. H. Yoon, M. S. Lah, *Cryst. Growth Des.* **2012**, *12*, 4186–4193; c) D. Sun, L. L. Han, S. Yuan, Y. K. Deng, M. Z. Xu, D. F. Sun, *Cryst. Growth Des.* **2013**, *13*, 377–385; d) L. Li, S. Wang, T. Chen, Z. Sun, J. Luo, M. Hong, *Cryst. Growth Des.* **2012**, *12*, 4109–4115; e) K. Koh, A. G. Wong-Foy, A. J. Matzger, *Angew. Chem. Int. Ed.* **2008**, *47*, 677–680; *Angew. Chem.* **2008**, *120*, 689; f) M. Yang, F. Jiang, Q. Chen, Y. Zhou, R. Feng, K. Xiong, M. Hong, *CrystEngComm* **2011**, *13*, 3971–3974; g) J. Cepeda, R. Balda, G. Beobide, O. Castillo, J. Fernández, A. Luque, S. Pérez-Yáñez, P. Román, *Inorg. Chem.* **2012**, *51*, 7875–7888; h) K. E. Knope, H. Kimura, Y. Yasaka, M. Nakahara, M. B. Andrews, C. L. Cahill, *Inorg. Chem.* **2012**, *51*, 3883.
- [7] a) S. Horike, S. Shimomura, S. Kitagawa, *Nat. Chem.* **2009**, *1*, 695–704; b) G. K. Kole, J. J. Vittal, *Chem. Soc. Rev.* **2013**, *42*, 1755–1775.
- [8] a) B. Chen, C. Liang, J. Yang, D. S. Contreras, Y. L. Clancy, E. B. Lobkovsky, O. M. Yaghi, S. Dai, *Angew. Chem. Int. Ed.* **2006**, *45*, 1390–1393; *Angew. Chem.* **2006**, *118*, 1418; b) C. Serre, C. Mellot-Draznieks, S. Surble, N. Audebrand, Y. Filinchuk, G. Férey, *Science* **2007**, *315*, 1828–1831; c) B. Xiao, P. J. Byrne, P. S. Wheatley, D. S. Wragg, X. Zhao, A. J. Fletcher, K. M. Thomas, L. Peters, J. S. O. Evans, J. E. Warren, W. Zhou, R. E. Morris, *Nat. Chem.* **2009**, *1*, 289–294; d) Z. Duan, Y. Zhang, B. Zhang, D. Zhu, *J. Am. Chem. Soc.* **2009**, *131*, 6934–6935; e) J. Seo, C. Bonneau, R. Matsuda, M. Takata, S. Kitagawa, *J. Am. Chem. Soc.* **2011**, *133*, 9005–9013.
- [9] a) M. Du, C. P. Li, C. S. Liu, S. M. Fang, *Coord. Chem. Rev.* **2013**, *257*, 1282–1305; b) M. Taddei, F. Costantino, A. Ienco, A. Comotti, P. V. Dau, S. M. Cohen, *Chem. Commun.* **2013**, 49, 1315–1317; c) H. Chevreau, T. Devic, F. Salles, G. Maurin, N. Stock, C. Serre, *Angew. Chem. Int. Ed.* **2013**, *52*, 5056–5060; d) X. L. Wang, Y. F. Bi, G. C. Liu, H. Y. Lin, T. L. Hu, X. H. Bu, *CrystEngComm* **2008**, *10*, 349–356.
- [10] V. A. Blatov, *IUCR CompComm Newsletter* **2006**, *7*, 4–38; *TOPOS v. 4.0* is available at <http://www.topos.ssu.samara.ru>.
- [11] A. L. Spek, *J. Appl. Crystallogr.* **2003**, *36*, 7–13.
- [12] a) Y. Cui, Y. Yue, G. Qian, B. Chen, *Chem. Rev.* **2012**, *112*, 1126–1162; b) M. D. Allendorf, C. A. Bauer, R. K. Bhakta, R. J. Houk, *Chem. Soc. Rev.* **2009**, *38*, 1330–1352; c) X. L. Wang, C. Qin, E. B. Wang, Y. G. Li, N. Hao, C. W. Hu, A. Xu, *Inorg. Chem.* **2004**, *43*, 1850–1856; d) L. Hou, Y. Y. Lin, X. M. Chen, *Inorg. Chem.* **2008**, *47*, 1346–1351; e) H. Y. Liu, H. Wu, J. F. Ma, Y. Y. Liu, B. Liu, J. Yang, *Cryst. Growth Des.* **2010**, *10*, 4795–4805; f) Z. Su, J. Fan, T. Okamura, M. S. Chen, S. S. Chen, W. Y. Sun, N. Ueyama, *Cryst. Growth Des.* **2010**, *10*, 1911–1922; g) D. Sun, Z. H. Yan, V. A. Blatov, L. Wang, D. F. Sun, *Cryst. Growth Des.* **2013**, *13*, 1277–1289; h) X. Zhang, L. Fan, Z. Sun, W. Zhang, D. Li, J. Dou, L. Han, *Cryst. Growth Des.* **2013**, *13*, 792–803; i) X. Zhang, L. Hou, B. Liu, L. Cui, Y. Y. Wang, B. Wu, *Cryst. Growth Des.* **2013**, *13*, 3177–3187.
- [13] a) L. Wen, Y. Li, Z. Lu, J. Lin, C. Duan, Q. Meng, *Cryst. Growth Des.* **2006**, *6*, 530–537; b) J. G. Lin, S. Q. Zang, Z. F. Tian, Y. Z. Li, Y. Y. Xu, H. Z. Zhu, Q. J. Meng, *CrystEngComm* **2007**, *9*, 915–921.
- [14] G. M. Sheldrick, *SHELXL-97: Program for Crystal Structure Refinement*, University of Göttingen, Germany, **1997**.
- [15] A. L. Spek, *Acta Crystallogr., Sect. A* **1990**, *46*, 194–201.

Received: February 22, 2014
Published Online: June 3, 2014